High-energy terahertz pulses from semiconductors pumped beyond the three-photon absorption edge

GY. POLÓNYI,[1,2] B. MONOSZLAI,[2,3] G. GÄUMANN,[4] E. J. ROHWER,[4] G. ANDRIUKAITIS,[5] T. BALCIUNAS,[5] A. PUGZLYS,[5] A. BALTUSKA,[5] T. FEURER,[4] J. HEBLING,[1,2] AND J. A. FÜLÖP[1,2,3,*]

[1]MTA-PTE High-Field Terahertz Research Group, 7624 Pécs, Hungary
[2]Institute of Physics and Szentágothai Research Centre, University of Pécs, 7624 Pécs, Hungary
[3]ELI-ALPS, ELI-Hu Nkft., 6720 Szeged, Hungary
[4]Institute of Applied Physics University of Bern, Bern 3012, Switzerland
[5]Photonics Institute, TU Wien, 1040 Vienna, Austria
*fulop@fizika.ttk.pte.hu

Abstract: A new route to efficient generation of THz pulses with high-energy was demonstrated using semiconductor materials pumped at an infrared wavelength sufficiently long to suppress both two- and three-photon absorption and associated free-carrier absorption at THz frequencies. For pumping beyond the three-photon absorption edge, the THz generation efficiency for optical rectification of femtosecond laser pulses with tilted intensity front in ZnTe was shown to increase 3.5 times, as compared to pumping below the absorption edge. The four-photon absorption coefficient of ZnTe was estimated to be $\beta_4 = (4 \pm 1) \times 10^{-5}$ cm^5/GW^3. THz pulses with 14 μJ energy were generated with as high as 0.7% efficiency in ZnTe pumped at 1.7 μm. It is shown that scaling the THz pulse energy to the mJ level by increasing the pump spot size and pump pulse energy is feasible.

References and links

1. T. Kampfrath, K. Tanaka, and K. A. Nelson, "Resonant and nonresonant control over matter and light by intense terahertz transients," Nat. Photonics **7**(9), 680–690 (2013).
2. E. A. Nanni, W. R. Huang, K.-H. Hong, K. Ravi, A. Fallahi, G. Moriena, R. J. D. Miller, and F. X. Kärtner, "Terahertz-driven linear electron acceleration," Nat. Commun. **6**, 8486 (2015).
3. L. Pálfalvi, J. A. Fülöp, G. Tóth, and J. Hebling, "Evanescent-wave proton postaccelerator driven by intense THz pulse," Phys. Rev. Spec. Top. Accel. Beams **17**(3), 031301 (2014).
4. J. Hebling, G. Almási, I. Kozma, and J. Kuhl, "Velocity matching by pulse front tilting for large area THz-pulse generation," Opt. Express **10**(21), 1161–1166 (2002).
5. H. Hirori, A. Doi, F. Blanchard, and K. Tanaka, "Single-cycle terahertz pulses with amplitudes exceeding 1 MV/cm generated by optical rectification in LiNbO₃," Appl. Phys. Lett. **98**(9), 091106 (2011).
6. S.-W. Huang, E. Granados, W. R. Huang, K.-H. Hong, L. E. Zapata, and F. X. Kärtner, "High conversion efficiency, high energy terahertz pulses by optical rectification in cryogenically cooled lithium niobate," Opt. Lett. **38**(5), 796–798 (2013).
7. J. A. Fülöp, Z. Ollmann, C. Lombosi, C. Skrobol, S. Klingebiel, L. Pálfalvi, F. Krausz, S. Karsch, and J. Hebling, "Efficient generation of THz pulses with 0.4 mJ energy," Opt. Express **22**(17), 20155–20163 (2014).
8. J. A. Fülöp, L. Pálfalvi, G. Almási, and J. Hebling, "Design of high-energy terahertz sources based on optical rectification," Opt. Express **18**(12), 12311–12327 (2010).
9. K. Ravi, W. R. Huang, S. Carbajo, X. Wu, and F. Kärtner, "Limitations to THz generation by optical rectification using tilted pulse fronts," Opt. Express **22**(17), 20239–20251 (2014).
10. C. Lombosi, G. Polónyi, M. Mechler, Z. Ollmann, J. Hebling, and J. A. Fülöp, "Nonlinear distortion of intense THz beams," New J. Phys. **17**(8), 083041 (2015).
11. F. D. J. Brunner, S.-H. Lee, O.-P. Kwon, and T. Feurer, "THz generation by optical rectification of near-infrared laser pulses in the organic nonlinear optical crystal HMQ-TMS," Opt. Mater. Express **4**(8), 1586–1592 (2014).
12. M. C. Hoffmann, K.-L. Yeh, J. Hebling, and K. A. Nelson, "Efficient terahertz generation by optical rectification at 1035 nm," Opt. Express **15**(18), 11706–11713 (2007).

13. F. Blanchard, L. Razzari, H.-C. Bandulet, G. Sharma, R. Morandotti, J.-C. Kieffer, T. Ozaki, M. Reid, H. F. Tiedje, H. K. Haugen, and F. A. Hegmann, "Generation of 1.5 microJ single-cycle terahertz pulses by optical rectification from a large aperture ZnTe crystal," Opt. Express **15**(20), 13212–13220 (2007).
14. K. L. Vodopyanov, "Terahertz-wave generation with periodically inverted gallium arsenide," Laser Phys. **19**(2), 305–321 (2009).
15. F. Blanchard, B. E. Schmidt, X. Ropagnol, N. Thiré, T. Ozaki, R. Morandotti, D. G. Cooke, and F. Légaré, "Terahertz pulse generation from bulk GaAs by a tilted-pulse-front excitation at 1.8 µm," Appl. Phys. Lett. **105**(24), 241106 (2014).
16. D. Peceli, P. D. Olszak, C. M. Cirloganu, S. Webster, L. A. Padilha, T. Ensley, H. Hu, G. Nootz, D. J. Hagan, and E. W. Van Stryland, "Three-photon absorption of GaAs and other semiconductors," in *Nonlinear Optics Technical Digest* (2013), paper NTu1B.6.
17. C. M. Cirloganu, P. D. Olszak, L. A. Padilha, S. Webster, D. J. Hagan, and E. W. Van Stryland, "Three-photon absorption spectra of zinc blende semiconductors: theory and experiment," Opt. Lett. **33**(22), 2626–2628 (2008).
18. M. Yin, H. P. Li, S. H. Tang, and W. Ji, "Determination of nonlinear absorption and refraction by single Z-scan method," Appl. Phys. B **70**(4), 587–591 (2000).
19. A. A. Said, M. Sheik-Bahae, D. J. Hagan, T. Wei, J. Wang, J. Young, and E. W. van Stryland, "Determination of bound-electronic and free-carrier nonlinearities in ZnSe, GaAs, CdTe, and ZnTe," J. Opt. Soc. Am. B **9**(3), 405–414 (1992).
20. V. Nathan, A. H. Guenther, and S. S. Mitra, "Review of multiphoton absorption in crystalline solids," J. Opt. Soc. Am. B **2**(2), 294–316 (1985).
21. H. H. Li, "Refractive index of ZnS, ZnSe, and ZnTe and its wavelength and temperature derivatives," J. Phys. Chem. Ref. Data **13**(1), 103–150 (1984).
22. M. Schall, M. Walther, and P. Uhd Jepsen, "Fundamental and second-order phonon processes in CdTe and ZnTe," Phys. Rev. B **64**(9), 094301 (2001).
23. K. Wynne and J. J. Carey, "An integrated description of terahertz generation through optical rectification, charge transfer, and current surge," Opt. Commun. **256**(4-6), 400–413 (2005).
24. J. Hebling, K.-L. Yeh, M. C. Hoffmann, B. Bartal, and K. A. Nelson, "Generation of high-power terahertz pulses by tilted-pulse-front excitation and their application possibilities," J. Opt. Soc. Am. B **25**(7), B6–B19 (2008).
25. M. Kunitski, M. Richter, M. D. Thomson, A. Vredenborg, J. Wu, T. Jahnke, M. Schöffler, H. Schmidt-Böcking, H. G. Roskos, and R. Dörner, "Optimization of single-cycle terahertz generation in LiNbO₃ for sub-50 femtosecond pump pulses," Opt. Express **21**(6), 6826–6836 (2013).
26. L. Pálfalvi, J. A. Fülöp, G. Almási, and J. Hebling, "Novel setups for extremely high power single-cycle terahertz pulse generation by optical rectification," Appl. Phys. Lett. **92**(17), 171107 (2008).
27. Z. Ollmann, J. A. Fülöp, J. Hebling, and G. Almási, "Design of a high-energy terahertz pulse source based on ZnTe contact grating," Opt. Commun. **315**, 159–163 (2014).
28. G. Andriukaitis, E. Kaksis, G. Polónyi, J. A. Fülöp, A. Baltuska, and A. Pugzlys, "220-fs 110-mJ Yb:CaF2 cryogenic multipass amplifier," in *CLEO:2015*, OSA Technical Digest (online) (Optical Society of America), (2015), paper SM1P.7.
29. S. A. Ku, C. M. Tu, W.-C. Chu, C. W. Luo, K. H. Wu, A. Yabushita, C. C. Chi, and T. Kobayashi, "Saturation of the free carrier absorption in ZnTe crystals," Opt. Express **21**(12), 13930–13937 (2013).
30. R. DeSalvo, A. A. Said, D. J. Hagan, E. W. van Stryland, and M. Sheik-Bahae, "Infrared to ultraviolet measurements of two-photon absorption and n₂ in wide bandgap solids," IEEE J. Quantum Electron. **32**(8), 1324–1333 (1996).
31. M. I. Bakunov and S. B. Bodrov, "Terahertz generation with tilted-front laser pulses in a contact-grating scheme," J. Opt. Soc. Am. B **31**(11), 2549–2557 (2014).
32. J. A. Fülöp, G. Polónyi, B. Monoszlai, G. Andriukaitis, T. Balciunas, A. Pugzlys, G. Arthur, A. Baltuska, and J. Hebling, "Highly efficient scalable monolithic semiconductor terahertz pulse source," Optica, in press.
33. M. Tsubouchi, K. Nagashima, F. Yoshida, Y. Ochi, and M. Maruyama, "Contact grating device with Fabry-Perot resonator for effective terahertz light generation," Opt. Lett. **39**(18), 5439–5442 (2014).
34. P. Malevich, G. Andriukaitis, T. Flöry, A. J. Verhoef, A. Fernández, S. Ališauskas, A. Pugžlys, A. Baltuška, L. H. Tan, C. F. Chua, and P. B. Phua, "High energy and average power femtosecond laser for driving mid-infrared optical parametric amplifiers," Opt. Lett. **38**(15), 2746–2749 (2013).
35. M. Hemmer, D. Sánchez, M. Jelínek, V. Smirnov, H. Jelinkova, V. Kubeček, and J. Biegert, "2-µm wavelength, high-energy Ho:YLF chirped-pulse amplifier for mid-infrared OPCPA," Opt. Lett. **40**(4), 451–454 (2015).
36. P. Kroetz, A. Ruehl, G. Chatterjee, A. L. Calendron, K. Murari, H. Cankaya, P. Li, F. X. Kärtner, I. Hartl, and R. J. D. Miller, "Overcoming bifurcation instability in high-repetition-rate Ho:YLF regenerative amplifiers," Opt. Lett. **40**(23), 5427–5430 (2015).
37. L. von Grafenstein, M. Bock, D. Ueberschaer, U. Griebner, and T. Elsaesser, "Picosecond 34 mJ pulses at kHz repetition rates from a Ho:YLF amplifier at 2 µm wavelength," Opt. Express **23**(26), 33142–33149 (2015).

1. Introduction

The application of intense THz pulses for strong-field control of matter [1], the acceleration and manipulation of electrons [2] and protons [3] opens up new perspectives in science and technology. The low-frequency part of the THz spectrum (0.1 to 2 THz) is particularly

suitable for applications involving charged particle beams, because the longer wavelength of THz pulses compares well with typical sizes of particle beams and bunches. Up to now, tilted-pulse-front pumping (TPFP) of optical rectification in lithium niobate (LN) [4] is the most efficient source in this spectral range [5–7]. The generation of THz pulses with more than 0.4 mJ energy was demonstrated with 0.77% efficiency [7]. However, further increase of the THz energy and field strength is challenging due to the limiting effects caused or strongly enhanced by the large pulse-front tilt (PFT) angle of about 63° [8–10], required for phase matching in LN. We note that THz spectra similar to those of LN were generated in the organic material HMQ-TMS [11].

Semiconductors, such as ZnTe and GaP are among the nonlinear materials most widely used for THz generation by optical rectification. Collinear phase matching is possible for example in ZnTe, GaP, and GaAs in the vicinity of 0.8 μm, 1 μm, and 1.5 μm wavelengths, corresponding to commonly used Ti:sapphire, Yb-doped, and Er-doped lasers, respectively. Conventionally, semiconductors were considered as less efficient for THz generation than LN [12]. The highest THz energy reported from a semiconductor source was 1.5 μJ [13], achieved in ZnTe with 3×10^{-5} efficiency. The reason for the low pump-to-THz energy conversion efficiency was strong two-photon absorption (2PA) at the pump wavelength of 0.8 μm, and the associated free-carrier absorption (FCA) at THz frequencies. However, recently, semiconductors were reconsidered for high-energy THz pulse generation [8]. At longer pump wavelengths, typically requiring TPFP, it is possible to suppress low-order multiphoton absorption (MPA) [14] and, consequently, FCA at THz frequencies. As a result, a higher pump intensity can be used and a higher THz generation efficiency can be expected. Recently, THz pulses with 0.6 μJ energy were generated at 5×10^{-4} efficiency by pumping GaAs at a wavelength of 1.8 μm, sufficiently long to suppress 2PA [15].

Here we present a comparative study of THz pulse generation in ZnTe, a direct band-gap semiconductor, pumped below and above the three-photon absorption (3PA) edge at 1.45 μm and 1.7 μm wavelengths, respectively. TPFP needs to be used at these wavelengths. The comparison is extended to GaP, having an indirect bandgap, pumped at 1.7 μm, above the 3PA edge. A highly efficient, high-energy THz pulse source is demonstrated by pumping ZnTe at 1.7 μm wavelength, sufficiently long to suppress both 2PA and 3PA. The results support the expectation that a new class of efficient THz sources based on semiconductors is coming up, scalable to mJ-level THz energies.

2. Simulations

ZnTe is a direct-bandgap semiconductor with a gap of 2.26 eV. Consequently, for pump wavelengths above 1.65 μm, the absorption edge for 3PA (Fig. 1(a)), only 4PA and higher-order MPA are effective. Wavelengths of MPA edges of various orders are indicated by symbols in Fig. 1(b) for a few different materials. Simulations of THz generation and experiments were carried out at pump wavelengths below and above the 3PA edge at 1.45 μm and 1.7 μm, respectively. Around 1.45 μm, where 3PA is still effective, a local minimum of the 3PA coefficient can be expected in ZnTe. Theoretical and experimental studies indicate that in zinc-blende type semiconductors such a minimum is at a 10% to 15% shorter wavelength than the 3PA edge [16,17]. A similar behavior is expected for GaP, where the indirect (direct) bandgap is 2.27 eV (2.48 eV).
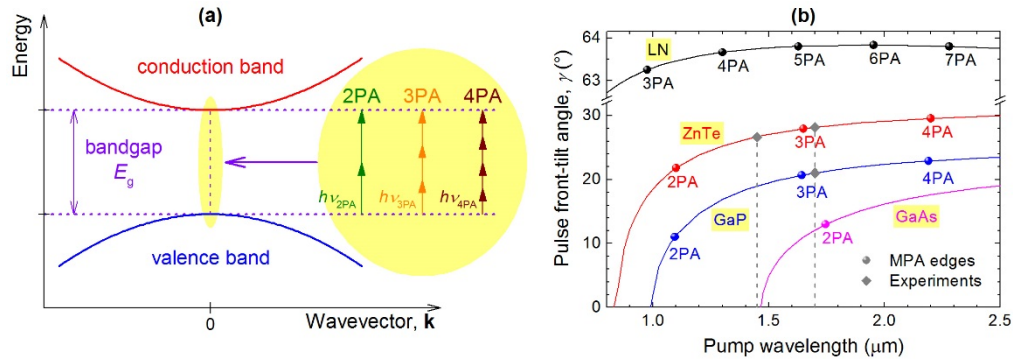
Fig. 1. (a) Schematic band structure of ZnTe having a direct bandgap and scheme of various MPA processes of order n pumped at the respective absorption edges of wavelengths $\lambda_{nPA} = c / \nu_{nPA}$, with c being the vacuum speed of light. (b) PFT angle versus pump wavelength for phase matching at 1 THz in LN and selected semiconductors. The symbols indicate the wavelengths of MPA edges of various orders. In case of GaP, the indirect bandgap is considered. The dashed vertical lines and the diamond symbols indicate the wavelengths and materials used in the experiment.

For the simulation of THz generation, the one-dimensional wave equation with the nonlinear polarization was solved in the spectral domain [8]. The model takes into account the variation of the pump pulse duration with propagation distance due to material and angular dispersions, the non-collinear propagation of pump and THz beams, and the absorption in the THz range due to phonon resonances. We note that in the literature contradictory data can be found on the nonlinear refractive index of ZnTe, ranging from $< 5 \times 10^{-15}$ cm^2/GW [18] to 1.2×10^{-13} cm^2/GW [14,19]. While nonlinear refraction (Kerr effect) could influence THz generation [9,14] for the larger value, we estimate its contribution negligible for the smaller. Further investigation could clarify its influence but it is beyond the scope of the present work.

FCA in the THz range, caused by 3PA of the pump, was taken into account in case of 1.45 μm pump wavelength. In the simulations, the estimated value of $\beta_3 = 1.8 \times 10^{-2}$ cm^3/GW^2 was taken for the 3PA coefficient of ZnTe. This value was obtained, in lack of known published data, from matching simulation results to experimental data (see Section 4). For GaP, the published value of $\beta_3 = 4.2 \times 10^{-2}$ cm^3/GW^2 was used [12,20]. In some of the simulations for ZnTe pumped beyond the 3PA edge at 1.7 μm, the estimated 4PA coefficient of $\beta_4 = 4 \times 10^{-5}$ cm^5/GW^3 was taken into account, obtained also from fit to experimental data shown in Section 4. The effect of higher-order pump absorption was not taken into account, due to lack of available data for the respective MPA coefficients.

Results of simulations clearly indicate that for obtaining high conversion efficiencies it is not sufficient to avoid only 2PA. Even 3PA can pose a serious limitation on the useful pump intensity, as shown in Fig. 2 by dashed curves for ZnTe and GaP in case of pump at 1.45 μm. Strong saturation of the THz generation efficiency is observed already at a low pump intensity of about 6 GW/cm^2 and 3 GW/cm^2 for ZnTe and GaP, respectively. The predicted efficiency is limited to about 2×10^{-3} and 1×10^{-3}, respectively. In contrast, for 1.7 μm pump and omitting 4PA, the THz generation efficiency increases linearly up to significantly higher intensities (solid lines in Fig. 2). Taking into account 4PA in ZnTe results in saturation of the THz generation efficiency even for 1.7 μm pump wavelength (short-dashed line in Fig. 2). However, the predicted maximum efficiency of 0.6% is about 3.4 times higher than in case of pump at 1.45 μm. About 16 GW/cm^2 pump intensity can be used in case of 1.7 μm pump. Similar behavior can be expected for GaP.
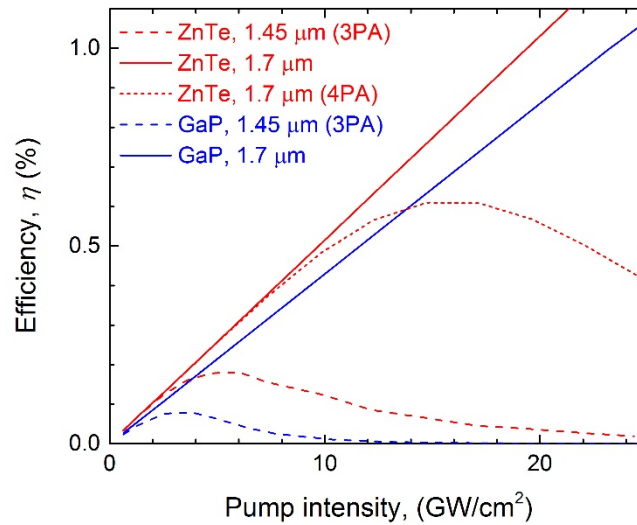
Fig. 2. Calculated THz generation efficiencies as function of pump intensity for ZnTe (red lines) and GaP (blue lines) for pump wavelengths set below (dashed lines) and above (solid and short-dashed lines) the 3PA edge. The order of MPA process taken into account is indicated in parentheses in the legend. 100 fs pump pulse duration and a crystal length of 2.9 mm was assumed. The phase matching frequency and the THz spectral peak were matched in each case.

The dependence of the phase-matching PFT angle on the pump wavelength is shown in Fig. 1(b) for the selected semiconductors and LN. The tilt angle can be calculated from optical and THz refractive index data (see [21], Li [22], Schall et al., and [23], Wynne et al. for ZnTe; for the other materials as referenced in [24], Hebling et al.). For example, the optical group index at 1.7 μm is 2.78 and the refractive index at 1 THz is 3.16, giving 28.1° for the PFT angle. In general, the PFT angle for semiconductors is about 30° or smaller, while for LN it is about 63°. A smaller tilt angle is very advantageous in TPFP for the following reasons: (i) it results in a smaller variation of the pulse duration (Fig. 3(a)) and the local conversion efficiency (Fig. 3(b)) during propagation through the nonlinear medium, thereby enabling to significantly increase the effective material length for THz generation [8]; (ii) the difference in crystal length across the pumped area is smaller, which reduces spatial non-uniformity in THz generation; (iii) it enables to reduce the distortion effects caused by the pulse-front tilting optics [8,25], thereby enabling a larger pump spot size in conventional TPFP setups using imaging; (iv) gratings with a smaller groove density can be used for TPFP, which is advantageous especially for the realization of a contact-grating THz source [26,27].

3. Experimental setup

Two different laser systems were used in the experiments for pumping the THz sources. For a comparative study of THz generation in ZnTe pumped at two different wavelengths of 1.45 μm and 1.7 μm and in GaP pumped at a wavelength of 1.7 μm, a commercial optical parametric amplifier (OPA) (Light Conversion, HE-TOPAS) was used. The OPA was driven by a Ti:sapphire laser system operating at 1 kHz repetition rate. In the following, this pump source will be referred to as "tunable OPA". The pulse length of the OPA output was about 100 fs. Up to 240 μJ and 360 μJ pump energy reached the THz generation crystal at 1.45 μm and 1.7 μm pump wavelengths, respectively. The pump spot size on the ZnTe and GaP prisms was about 2.6×2.0 mm^2 and 2.4×2.2 mm^2 (horizontal × vertical) at 1/e^2 level, respectively.
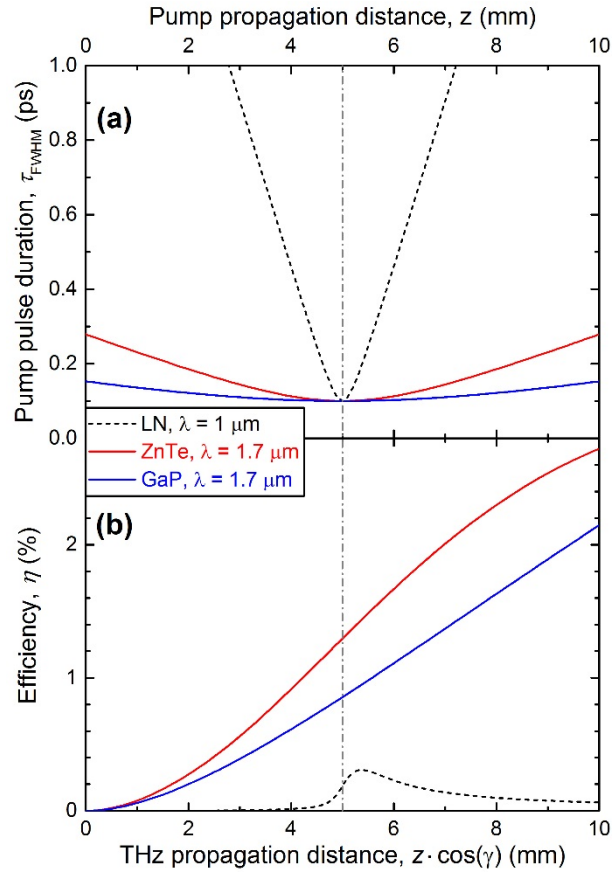
Fig. 3. (a) Pump pulse duration as function of the pump propagation distance z for LN, ZnTe, and GaP crystals. For LN a pump wavelength of 1 μm, for ZnTe and GaP 1.7 μm were chosen. The position of minimum (Fourier limited) pulse duration was arbitrarily set by pre-chirp to 5 mm in all cases (indicated by the vertical dashed-dotted line). (b) THz generation efficiency as a function of THz propagation distance. Parameters used in the simulations: 100 fs Fourier limited pump pulse duration with a pre-chirp at $z = 0$, pump intensity of 9 GW/cm^2, and phase matching at 1 THz.

For the generation of high-energy THz pulses in ZnTe, pump pulses were generated in a home-built supercontinuum-seeded four-stage OPA system, delivering 144-fs, 2.7-mJ pulses centered at 1.7 μm wavelength. This pump source will be referred to as "high-energy OPA". The high-energy OPA was driven at 1.03 μm wavelength by a cryogenically cooled Yb:CaF$_2$ chirped-pulse amplification laser system [28], consisting of an oscillator, a stretcher, a regenerative amplifier, a multipass power amplifier, and a compressor. The system delivered 200 fs pulses with 90 mJ pulse energy at 50 Hz repetition rate. The pump spot size on the ZnTe prism was about 4.4 × 3.2 mm^2 (horizontal × vertical) at 1/e^2 level.

The experimental setup is shown in Fig. 4. THz pulses were generated in (110)-oriented ZnTe and GaP prisms at room temperature (inset of Fig. 4), using conventional pulse-front tilting setups [4], consisting of a grating and a lens and optimized for minimum imaging distortions [8]. For ZnTe a 600 lines/mm, for GaP a 450 lines/mm grating was used. A half-wave plate rotated the horizontal polarization of the pump light, diffracted off the grating, to vertical, parallel to the [$1\bar{1}1$] axis of the crystals (inset of Fig. 4). The focal length of the fused silica lens was 200 mm.
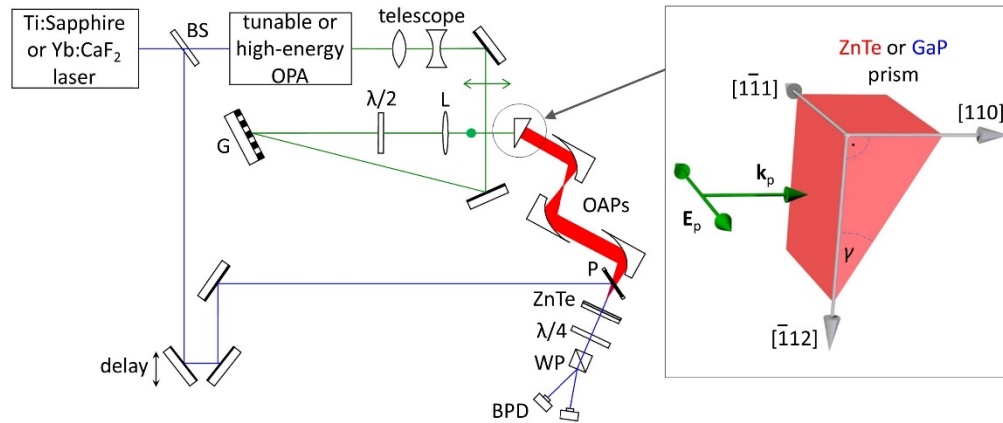
Fig. 4. Experimental setup. BS: beam splitter, G: grating, λ/2: half-wave plate, L: lens, OAPs: off-axis parabolic mirrors, P: pellicle beam splitter, ZnTe: sandwiched ZnTe crystal for electro-optic sampling, λ/4: quarter-wave plate, WP: Wollaston prism, BPD: balanced photodiodes. The inset shows the orientation of crystal axes in the semiconductor prisms.

The THz pulse energy was measured by a calibrated pyroelectric detector (Gentec, QS9-THZ-BL). A Teflon plate blocked the infrared pump and transmitted only the THz radiation to the detector. The voltage signal of the detector was fed to a storage oscilloscope and the THz energy W_{THz} was calculated from the voltage modulation V_m of the recorded trace according to $W_{THz} = CV_m\tau / S$, where the sensitivity $S = 1.2\,kV/W$ was obtained from factory calibration, while the correction factor $C \approx 1$ and the time constant $\tau = 5.1\,\text{ms}$ were determined from fitting of the recorded trace.

In the case of experiments aiming at the generation of high-energy THz pulses pumped by the high-energy OPA, the waveform was measured by electro-optic sampling (EOS). A small fraction of the 200-fs, 1.03-µm pump pulses was used for sampling. THz-induced birefringence was measured by conventional balanced-detection technique in a 0.1 mm thick, (110)-cut ZnTe crystal, contacted to a 2 mm thick differently cut inactive substrate of the same material. As the sampling pulses were relatively long, which distorted the measured spectrum, Fourier transform spectroscopy was also used. For this purpose, the field autocorrelation was measured with a Michelson interferometer, containing a 4 mm thick silicon beam splitter and a pyroelectric energy meter as detector. The THz spectrum was obtained by Fourier transformation of the interferogram.

4. Results and discussion

In the first of the two measurement series, a comparative study of THz generation in ZnTe pumped at 1.45 µm and 1.7 µm, and GaP pumped at 1.7 µm wavelength was carried out. Pump pulses were delivered by the tunable OPA. The measured THz energy and THz generation efficiency as functions of pump energy and intensity, respectively, are shown in Fig. 5. In the case of 1.45 µm pump a maximum efficiency of about 4×10^{-4} is reached at 6 GW/cm^2 pump intensity, which indicates the onset of 3PA. At higher intensities the efficiency was observed to decrease slowly. At about 14 GW/cm^2 pump intensity the efficiency starts to increase again, which can be caused by the saturation of 3PA. We note that a similar behavior, owing to the saturation of 2PA, was observed in ZnTe at 0.8 µm pump wavelength [29]. At 1.7 µm, where only 4PA and higher-order absorption were effective, the efficiency was increasing up to a maximum of about 1.4×10^{-3} at 13.5 GW/cm^2 intensity, followed by a decrease. This efficiency is up to 3.5 times higher than in case of 1.45 µm pump wavelength, owing to the elimination of 3PA. A saturation of the efficiency at the level of about 6×10^{-4} was observed for GaP pumped at 1.7 µm. This is slightly lower than that of

ZnTe, and can be explained by the smaller nonlinear coefficient of GaP and possibly by a larger 4PA coefficient.
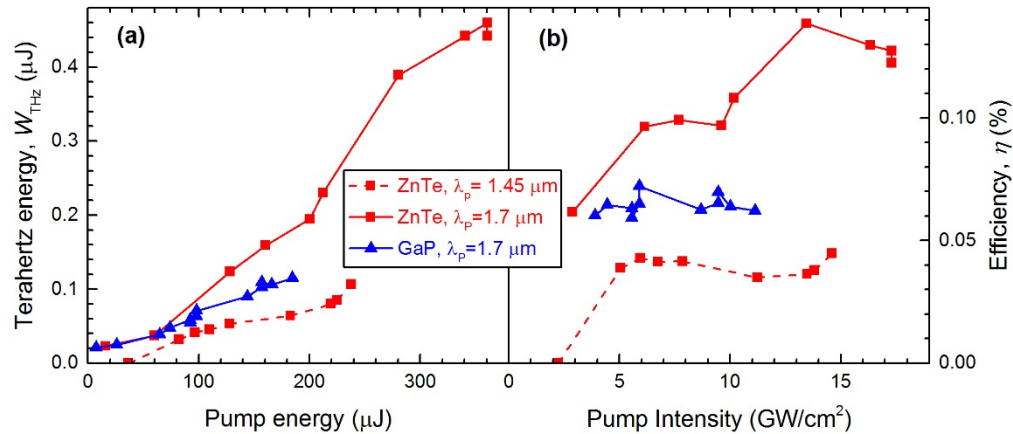

Fig. 5. THz energy as function of pump energy (a) and THz generation efficiency as function of pump intensity (b) for ZnTe pumped at 1.45 μm and 1.7 μm wavelengths, and for GaP pumped at 1.7 μm. The pump pulse duration from the tunable OPA was about 100 fs.

Comparing the measured efficiencies for ZnTe in Fig. 5(b) to the corresponding simulations in Fig. 2 shows that the simple model used here can qualitatively predict the efficiency maximum caused by 3PA at 1.45 μm pump and by 4PA at 1.7 μm pump. However, the measured peak efficiencies are smaller by about a factor of four than the calculated ones. This discrepancy could be caused by the small pump spot size in the experiment, which limits the interaction length. A much better prediction of the peak efficiency is found in case of a larger spot size, as discussed below.

In the second measurement series, the pump source was the high-energy OPA, enabling to use significantly higher pump energy at 1.7 μm wavelength. The measured THz energy and THz generation efficiency as functions of pump energy and intensity are shown in Fig. 6. The larger pump energy enabled a larger pump spot and resulted in significantly increased THz energy and efficiency. THz pulses with up to 14 μJ energy were observed (Fig. 6(a)), generated with 0.5% efficiency. For comparison, the previously reported highest THz pulse energy from a semiconductor source was 1.5 μJ [13]. As high as 0.7% maximum conversion efficiency was achieved at about 15 GW/cm² pump intensity (Fig. 6(b)), corresponding to 6.6 μJ THz energy. The decreasing efficiency above this pump level can be caused by 4PA. The achieved maximum efficiency is 14 times higher than the highest value reported previously from any semiconductor source [15], and the enormous 220 times higher than the highest previously reported value for a ZnTe source [13]. In [15], Blanchard et al., GaAs was pumped above the 2PA, but below the 3PA edge, while in [13], Blanchard et al., ZnTe was collinearly pumped at 0.8 μm, which caused strong 2PA. Our control measurement at 0.8 μm pump wavelength using a 2 mm thick (110)-cut ZnTe plate, pumped by 100-fs pulses at 15 GW/cm² intensity, resulted in only 5×10^{-6} efficiency. This is about five times lower than that in [13] at the same pump intensity. The difference between efficiencies could be caused by the different pump pulse durations (30 fs in [13]) and the difference in detector calibrations.
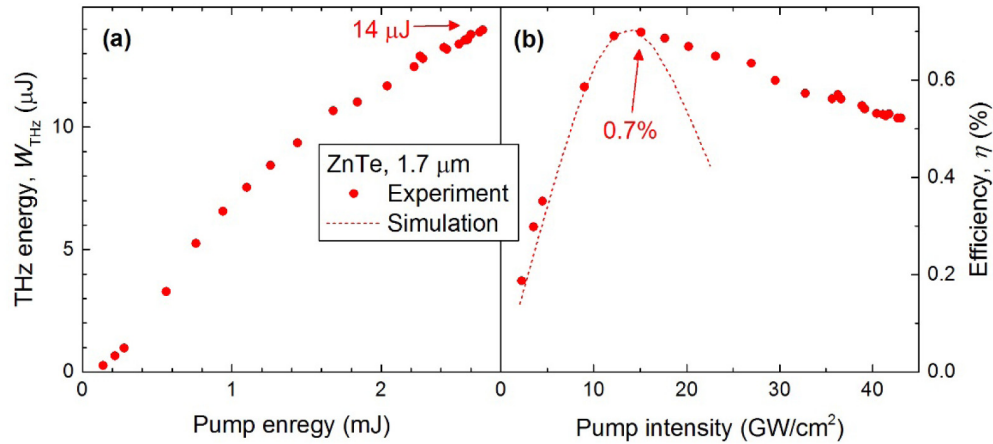
Fig. 6. THz energy as function of pump energy (a) and THz generation efficiency as function of pump intensity (b) for ZnTe pumped by the high-energy OPA at 1.7 µm. The pump pulse duration from the high-energy OPA was about 144 fs. The dashed curve in (b) is a result of simulation taking into account 4PA.

The observed saturation of the THz generation efficiency in ZnTe can be attributed to FCA due to 4PA of the pump at 1.7 µm. Both measurement series at 1.7 µm pump, presented in Figs. 5 and 6, c of $\beta_4 = (4 \pm 1) \times 10^{-5}$ cm^5/GW^3 (see Section 2). This value was obtained by fitting simulation results to the experimental data of Fig. 6 in terms of the pump intensity at which the efficiency maximum occurs. However, the simulation reproduces, with less than 15% relative deviation, also the measured peak value of the efficiency (the dashed curve in Fig. 6(b) has been rescaled to compensate for this small deviation). The slower roll-off of the measured efficiency, as compared to the simulated one, may be attributed to saturation of 4PA and needs further investigation beyond the scope of the present work. For comparison, the relatively small value of $\beta_4 = 10^{-7}$ cm^5/GW^3 was estimated for LN pumped at 1.03 µm in [12], Hoffmann et al. This is in agreement with general trends such as increasing nonlinearity with decreasing bandgap energy [30]. The observed onset of 4PA at about 14 GW/cm^2 pump intensity in ZnTe, as compared to the observed onset of 3PA at about 6 GW/cm^2, indicates that avoiding 3PA enables to efficiently use more than two times higher pump intensity. This larger pump intensity was essential for achieving the unprecedented high efficiencies up to 0.7%. The intensity range of data for GaP is more limited in Fig. 5. However, they suggest a 4PA coefficient for GaP larger than that of ZnTe, in accordance with the ratios of the respective 3PA coefficients (see Section 2).

EOS revealed a nearly single-cycle THz waveform (Fig. 7(a)). In order to avoid distortions due to the relatively long sampling pulses, Fourier transform spectroscopy was used to measure the THz spectrum. For this purpose, the field autocorrelation (AC, Fig. 7(b)) was recorded with a Michelson interferometer. The THz spectrum (Fig. 7(c)), obtained by Fourier transformation of the interferogram, has a maximum of the spectral intensity at 0.7 THz and the spectrum extends up to about 2.0 THz. A reasonably good qualitative agreement with the simulated spectrum was found.

Table 1 summarizes THz pulse generation results with semiconductor nonlinear materials reported in this work and compares them to previously published data. The data are classified according to the lowest-order effective MPA, determined by the pump photon energy compared to bandgap. Comparison of the data with 2PA and 3PA as the lowest-order effective MPA shows that eliminating 2PA enables the increase of THz generation efficiency by more than one order of magnitude. Comparing the data of this work with 3PA and 4PA as the lowest-order effective MPA, respectively, indicates that an additional 3.5 × increase can

be gained by eliminating also 3PA. Semiconductors can compete in efficiency even with LN when optimal conditions (pump wavelength, intensity, pulse duration, material thickness) are applied. The significantly smaller effective nonlinear coefficient of semiconductors, as compared to that of LN, can be compensated for by a larger effective interaction length, enabled by the much smaller PFT angle. Furthermore, a small tilt angle is very advantageous for the realization of a semiconductor contact-grating THz source with exceptionally favorable energy scaling properties [26,27,31,32].
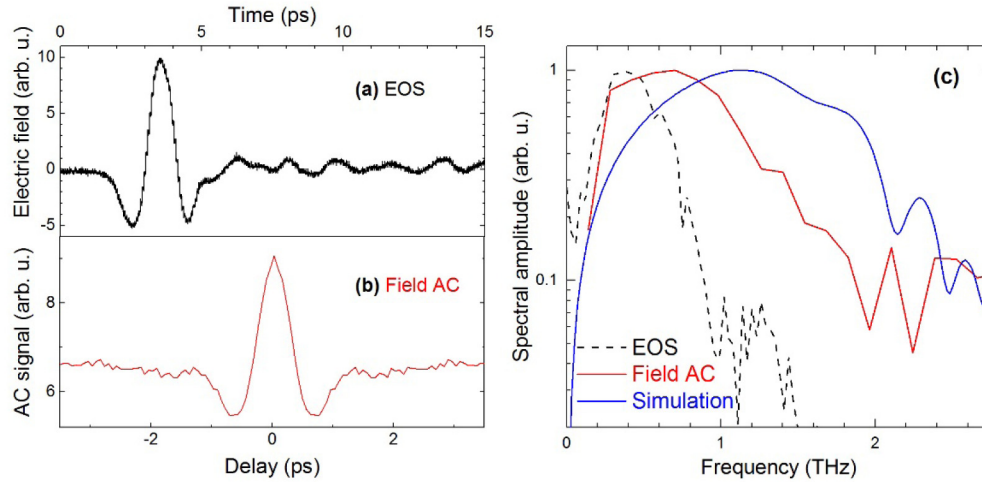

Fig. 7. (a) Temporal waveform of THz pulses generated in ZnTe, pumped at 1.7 µm by the high-energy OPA, and measured by EOS at maximum pump energy. (b) Field AC of THz pulses measured by a Michelson interferometer at maximum pump energy. (c) Spectral amplitude of THz pulses obtained by Fourier transformation of EOS data (black line) and field AC (red line), and from simulation (blue line).

Table 1. Comparison of THz generation results. Data are classified according to the lowest-order effective MPA, determined by the pump photon energy compared to bandgap. λ_{pump} : pump wavelength, γ : PFT angle. The efficiency and THz pulse energy values for this work refer to data measured with the high-energy OPA (144 fs pump pulse duration), while values in parentheses refer to those with the tunable OPA (100 fs pulse duration).

Lowest-order effective MPA	2PA	3PA		4PA		
Material	ZnTe	ZnTe	GaAs	ZnTe	GaP	LN
Ref.	[13]	This work	[15]	This work	This work	[7]
λ_{pump} [µm]	0.8	1.45	1.8	1.7	1.7	1.03
γ	0° (collinear)	27°	14°	28°	21°	63°
Max. efficiency [$\times 10^{-5}$]	3.1	(40)	50	700 (140)	(60)	770
Max. THz energy [µJ]	1.5	(0.11)	0.6	14 (0.46)	(0.11)	436

5. Conclusion

It was demonstrated both numerically and experimentally that semiconductor materials, pumped at an infrared wavelength sufficiently long to suppress 2PA and 3PA, offer a new route to efficient generation of THz pulses with high-energy. The suppression of FCA at THz frequencies, associated with low-order MPA, enables high-intensity pumping, which

consequently leads to unprecedentedly high THz generation efficiencies. At such long pump wavelengths TPFP is needed for phase matching.

Using a ZnTe TPFP source, pumped at 1.7 μm wavelength, as high as 0.7% THz generation efficiency was demonstrated. This is 14 times higher than the highest previously reported value for any semiconductor [15], and the vast 220 times higher than previously reported for ZnTe [13]. Such a high efficiency is comparable to that achieved with LN at high pulse energies [7]. Furthermore, it was shown that the THz generation efficiency in semiconductors can be increased by more than one order of magnitude in case of pumping beyond the 2PA edge, as compared to pumping below it [13]. The measurements also indicate the saturation of 3PA. Further increase of the efficiency by a factor of 3.5 was observed in case of pumping above the 3PA edge, as compared to pumping below it. An estimation of $\beta_4 = (4\pm1)\times10^{-5}$ cm^5/GW^3 for the 4PA coefficient was given for ZnTe.

THz pulses with as high as 14 μJ energy were generated, $9 \times$ higher than the highest previously reported value for semiconductors [13]. Further increase of the THz pulse energy to the mJ level can be expected by increasing the pump spot size to a few cm and scaling the pump pulse energy to the 100-mJ level, in combination with the scalable monolithic contact-grating technology [26,27,31,32]. Such new THz sources, in combination with novel efficient infrared pump sources in the 1.7 to 2.5 μm wavelength range based, for example, on Holmium laser technology [34–37], opens new perspectives for THz high-field applications. These range from strong-field control of matter to compact sources of high-energy particles and X-ray beams, key technologies in medicine and materials science.

Funding

Acknowledgments